Article

A New Synthesis Approach for Carbon Nitrides: Poly(triazine imide) and Its Photocatalytic Properties

Leonard Heymann,[†] Björn Schiller,[†] Heshmat Noei,[‡] Andreas Stierle,[‡,§] and Christian Klinke[*,†,‖]

[†]Institute of Physical Chemistry, University of Hamburg, Grindelallee 117, 20146 Hamburg, Germany
[‡]DESY NanoLab, Deutsches Elektronen-Synchrotron DESY, 22607 Hamburg, Germany
[§]Physics Department, University of Hamburg, 20355 Hamburg, Germany
[‖]Department of Chemistry, Swansea University, Singleton Park, Swansea SA2 8PP, United Kingdom

S Supporting Information

ABSTRACT: Poly(triazine imide) (PTI) is a material belonging to the group of carbon nitrides and has shown to have competitive properties compared to melon or g-C_3N_4, especially in photocatalysis. As most of the carbon nitrides, PTI is usually synthesized by thermal or hydrothermal approaches. We present and discuss an alternative synthesis for PTI which exhibits a pH-dependent solubility in aqueous solutions. This synthesis is based on the formation of radicals during electrolysis of an aqueous melamine solution, coupling of resulting melamine radicals and the final formation of PTI. We applied different characterization techniques to identify PTI as the product of this reaction and report the first liquid state NMR experiments on a triazine-based carbon nitride. We show that PTI has a relatively high specific surface area and a pH-dependent adsorption of charged molecules. This tunable adsorption has a significant influence on the photocatalytic properties of PTI, which we investigated in dye degradation experiments.
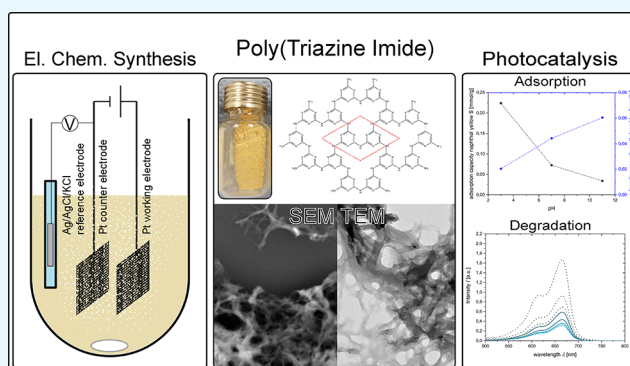
INTRODUCTION

Carbon nitrides have emerged as a new class of semiconducting materials with a large variety of possible applications. Because photocatalytic water splitting has been reported for these compounds in 2009,[1] most of them were prepared by thermal or hydrothermal synthesis leading in the formation of melon[2,3] (often referred as g-C_3N_4),[4−9] poly melamine,[10,11] poly-(heptazine imide),[12,13] or poly(triazine imide) (PTI).[14−18] Kessler et al. discuss in their review the differences of these structures and their promising properties, especially in photocatalysis.[19] In the literature, it was shown that carbon nitrides are capable of reducing carbon dioxide,[20−25] splitting water,[1,20,26−29] degrading organic pollutants such as dyes[6,12,22,30−32] under illumination in the visible range, as well as having a high sensitivity in sensing applications,[31,33−37] and catalyzing organic reactions.[38−42]

Different approaches have been used to improve the photocatalytic properties of these carbon nitrides. Ong et al. give a good overview over the so-far published carbon nitrides and their modifications.[43] By elemental doping,[44−47] copolymerization,[48,49] templating,[50,51] or forming composites especially with nanocrystals,[52−57] it was possible to further extend the number of applications in photocatalysis, and even dark photocatalysis has been reported recently by Lau et al.[58] Being restricted to thermal and hydrothermal synthesis limits the

variety in the above mentioned approaches. Therefore, it is important to discuss alternative strategies for the synthesis to further improve the properties of carbon nitrides.

In 2015, Lu et al. reported the synthesis of graphitic carbon nitride nanosheets using a new electrochemical approach and showed the peroxidase-like activity of those nanosheets.[59] In a new experimental setup with differences in the subsequent washing procedure, we were able to obtain a carbon nitride material either in solution [aqueous sodium hydroxide solution at pH 13 and dimethyl sulfoxide (DMSO)] or as suspension (water at neutral pH) that can be freeze-dried, yielding the powdery product. We applied different techniques in solid state, such as X-ray photoelectron spectroscopy (XPS), X-ray diffraction (XRD), and Fourier transform infrared spectroscopy (FTIR), and also liquid-state techniques such as two-dimensional $^1H−^{15}N$ NMR spectroscopy to identify the product of the synthesis as PTI. Reasonable yields could be achieved, and the as-described synthesis is facile and safe compared to molten salt synthesis, which were conducted under high pressure.[14−18] Besides the thorough characterization, we were able to demonstrate and investigate PTI adsorption behavior for
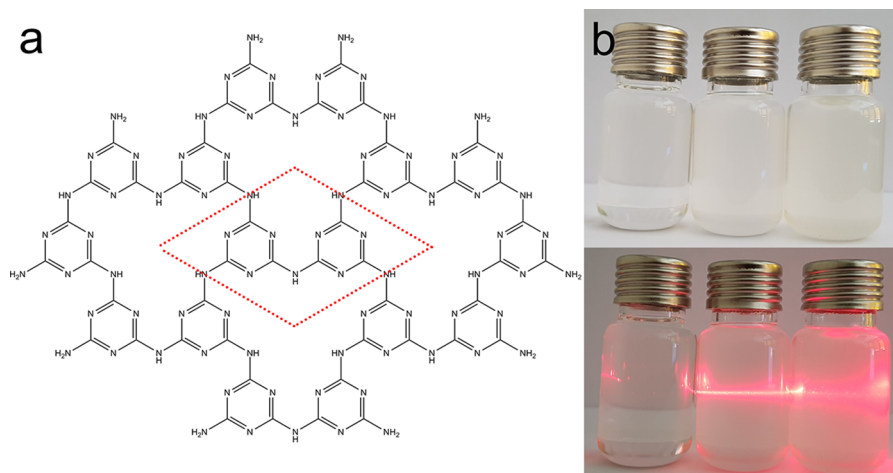
Figure 1. Structure of a single plane of PTI and its unit cell (red) (a). Picture of PTI at different pH values (from left to right: pH 13, pH 1, and pH 7) (b). At pH 1 and pH 7, a nonstable suspension is obtained, while at pH 13 a solution is formed (top). The lower image shows the Tyndall effect at pH 1 and pH 7. At pH 13, the Tyndall effect cannot be observed (bottom).

charged molecules by the examples of naphthol yellow S (NYS) (anionic) and methylene blue (MB) (cationic). Additionally, we demonstrated its capability in photocatalytic dye degradation of MB, and we further investigated the active species in these processes.

RESULTS AND DISCUSSION

The as-prepared product is proposed to be PTI. A schematic of the molecular structure is shown in Figure 1a. In the following passages, different characterization methods are combined to confirm this hypothesis. In general, the yellowish-brown product can be obtained in solution or in suspension, depending on the amount of sodium hydroxide in the synthesis. Figure 1b shows PTI in aqueous solutions at different pH values. The Tyndall effect describes the scattering of an incident beam by small particles. Therefore, the beam is observable not only in the direction of propagation but also at different observation angles. The absence of this effect at pH 13 indicates the formation of a solution, whereas at pH 1 and pH 7 a suspension is formed. Even after being synthesized and washed, PTI can be either dissolved in aqueous solution because of the formation of the PTI anion as well as being again precipitated by protonation. We assume that the imide group can be deprotonated by the addition of a base, for example, sodium hydroxide. The deprotonated and negatively charged PTI can be processed and analyzed in solution, which opens the possibility of a wide range of characterization techniques, for example, liquid-state NMR spectroscopy. The addition of an acid such as hydrochloric acid results in the precipitation of PTI. This process does not change the observed properties of PTI. Besides, Miller et al. recently described the spontaneous dissolution of PTI in DMSO.[60] We were able to reproduce these results and observed a solubility of PTI at room temperature of 9.1 mg/mL and 10.2 mg/mL in DMSO and sodium hydroxide solution at pH 13, respectively. The solubility was determined by preparing a saturated solution of PTI in each of the solvents, filtering the supernatant with a syringe filter followed by the evaluation of the mass of PTI in a defined volume.

Lu et al. described the formation process of their graphitic carbon nitride as a coupling of oxidized melamine radicals.[59] These radicals were formed by the reaction of melamine with

radical species emerging during the electrolysis of water, namely hydroxyl and superoxide radicals. These radicals are in situ formed at voltages exceeding the standard potentials for electrolysis of water of 1.23 V plus the overpotential. A similar approach has been described for carbon nanostructures prepared using electrochemical exfoliation by Lu et al.[61] It can be observed that the colorless solution of melamine in water turns yellowish during the reaction. We noticed that this change of color takes place at the anode, which leads us to the assumption that radicals, which are evolving during the oxidation of water, may be the main reactive species in this reaction. To further prove that assumption, we studied the formation of hydroxyl radicals. To do so, terephthalic acid was dissolved in 1 M sodium hydroxide solution. The acid has been added next to the anode. Aliquots were taken after certain time intervals. The formation of 2-hydroxyterephthalic acid was observed by detecting the emission at 425 nm. The emission spectra are shown in Figure S2. The influence of the as-formed hydroxyl radicals was proven through conducting the regular experiment in the presence of terephthalic acid. It was observed that the color change appears later, and less PTI is yielded.

Characterization. In the following section, different methods are combined to identify PTI as the product of the above described reaction and its physical properties are discussed.

To determine the morphology of PTI, transmission electron microscopy (TEM) and scanning electron microscopy (SEM) images were evaluated (Figure 2). Porous networks of PTI which are composed of loose ribbonlike fragments can be observed. These fragments are up to 500 nm long and up to 80 nm wide. In selected area electron diffraction, only broad rings with low intensity can be observed in very dense areas. Therefore, we assume that these PTI ribbons have small crystalline domains and are not single crystalline. The significant porosity of the networks is confirmed by the specific surface of 96 m^2 g^{-1} found by multipoint Brunauer−Emmett−Teller (BET) isotherm analysis (adsorption/desorption isotherms as well as a multipoint BET fit are shown in Figure S3) and is relatively high compared to that of other carbon nitride materials.[20,22,29]

When PTI is dissolved in DMSO, a change in the morphology is observed. The SEM and TEM images are
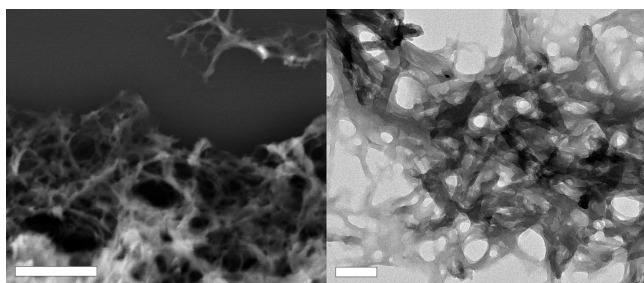
Figure 2. SEM and TEM images of the obtained PTI. The ribbonlike fragments arrange in loose networks with a high porosity. The scale bars in the SEM and TEM images are 500 and 100 nm, respectively.

shown in Figure S4. The obtained structures exhibit a two-dimensional morphology.

Despite the above-mentioned small domain sizes, two characteristic reflexes can be observed in powder XRD of the as-obtained product. The reflex at 27.66° is related to the (002) stacking of conjugated aromatic systems. The calculated interlayer distance is found to be 3.22 Å. The values for tri-s-triazine based carbon nitride are 27.4° and 3.26 Å.[1] The less intense reflex at 10.6° is labeled as (100) and is defined by the distance of 8.33 Å. This distance is found in the repeating unit in plane, more precisely in the periodicity of the pores formed by the s-triazine subunits. The shift in the reflex of the s-triazine based carbon nitride compared to the tri-s-triazine based carbon

nitride (13.0° and 6.81 Å)[1] is clearly observable and is explained through the smaller unit cell of the latter. Figure 3a shows the XRD pattern of the proposed s-triazine based structure shown in Figure 1. The distance of 8.33 Å shows a slight shift compared to values found for PTIs with intercalated metal ions synthesized using hydrothermal approaches.[15,62,63] The broadening of the reflexes indicates small crystal sizes. Using the Scherrer equation, a crystal size of around 9 nm is found for the analysis of the (100) reflex. The crystal size found for the reflex (002) at 27.66 Å is 14 nm. We explain the absence of higher-order reflexes by the size of the crystals, which is low compared to PTI prepared by molten salt synthesis. Wirnhier et al. report sizes of up to 60 nm.[14]

To confirm our hypothesis, the elemental composition was evaluated through combustion (carbon, nitrogen, and hydrogen) and pyrolysis analysis (oxygen). The determined values are presented in Table 1.

Table 1. Amounts of Carbon, Nitrogen, Hydrogen, and Oxygen Found in the Sample by Combustion and Pyrolysis Analysis

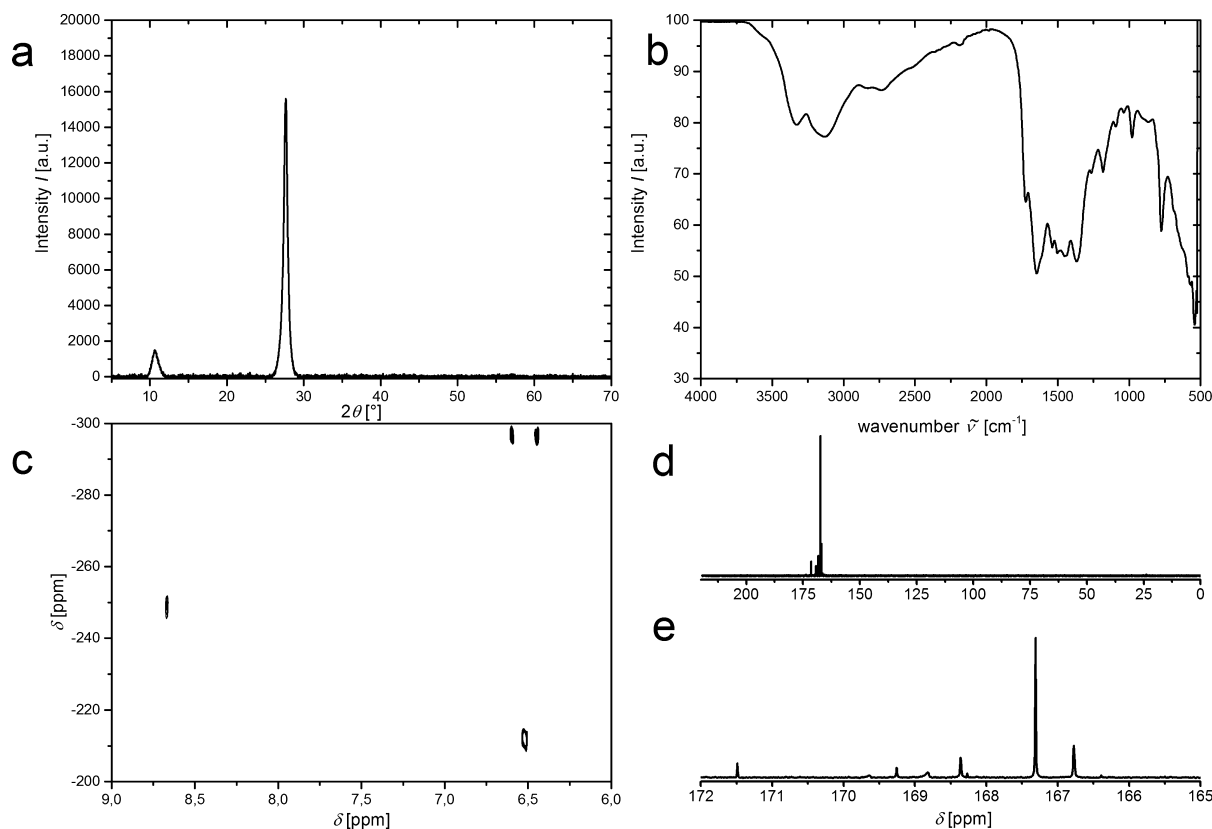|	C mass % (atomic %)	N mass % (atomic %)	H mass % (atomic %)	O mass % (atomic %)
combustion analysis	26.11 (20.84)	47.79 (32.71)	3.67 (34.91)	
pyrolysis analysis				19.27 (11.54)

Figure 3. XRD pattern of PTI shows two characteristic reflexes at 10.6° and 27.66°, which are related to an in-plane periodicity (100) and interlayer stacking (002), respectively (a). FTIR spectrum of PTI recorded between 500 and 4000 cm^{-1}. The spectrum shows characteristic absorptions at 775 cm^{-1}, between 1100 and 1700 cm^{-1}, especially at 1260 cm^{-1}, and around 3130 cm^{-1} and 3330 cm^{-1} (b). ^{1}H, ^{15}N HMBC NMR spectrum of PTI in DMSO. Signals are observed at −212.2, −249.5, and −296.4 ppm with respect to nitromethane. These signals can be assigned to the central ring nitrogen and the bridging imide and amine nitrogen, respectively (c). ^{13}C NMR spectrum of PTI in DMSO. Signals are observed between 166.7 and 171.5 ppm. These peaks can be assigned to the carbon atoms in triazine and heptazine rings (d,e).
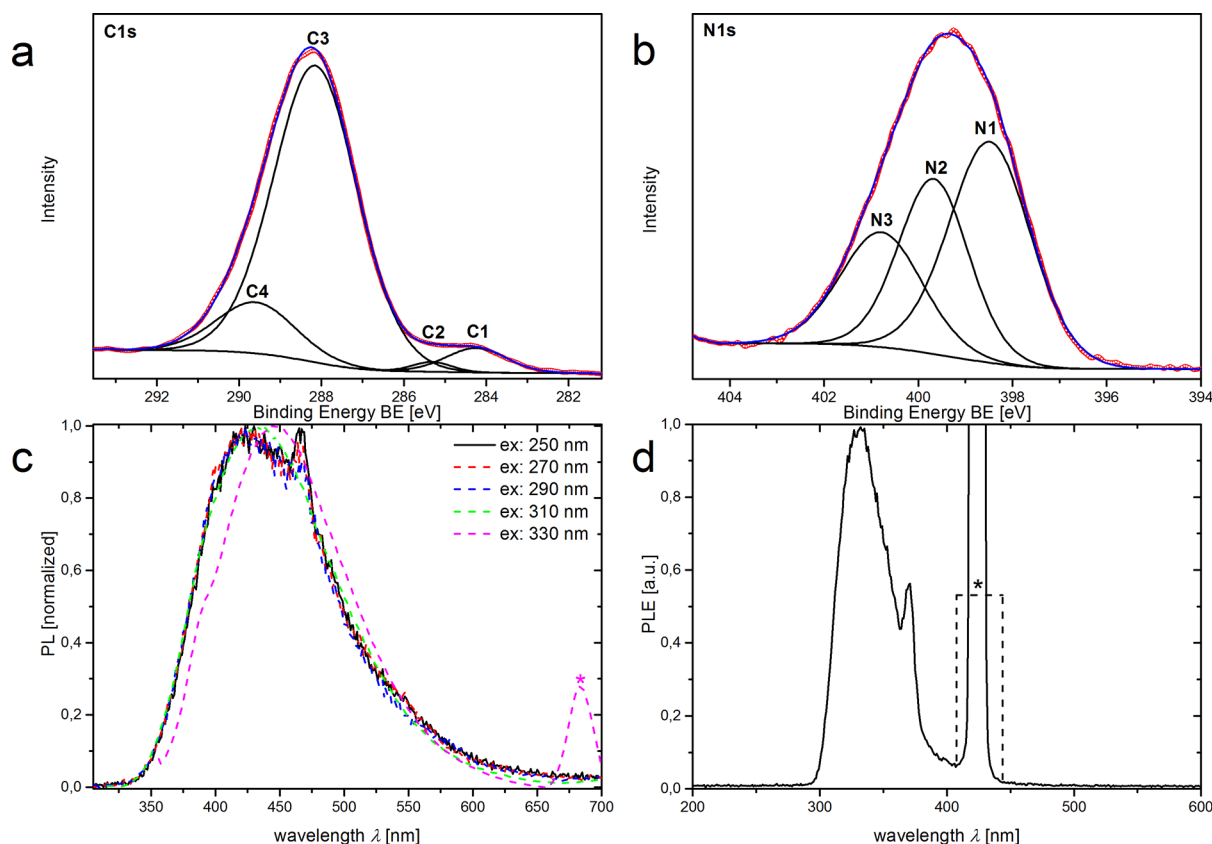
Figure 4. C 1s (a) and N 1s (b) XP spectra of PTI. Red circles denote the measured data and the fits are represented by blue curves. With an increasing excitation wavelength, the photoluminescence (PL) spectra of PTI in NaOH solution (pH 12) shows a red shift in the PL (c). The PL excitation (PLE) spectrum shows two maxima. The first and more intense is found at 330 nm and is contributed by PTI; the second at 370 nm is assigned to Raman scattering of water (d). The asterisks in (c,d) mark measurement artifacts at double excitation wavelength and the excitation wavelength, respectively.

For an integer amount of carbon, a sum formula of $C_3N_{4.7}O_{1.7}H_5$ is calculated. These values are in good agreement with the values of $C_3N_{4.5}H_{1.5}$ given for the unit cell of PTI defined in Figure 1a. The nonconformity of the values found for hydrogen and oxygen can be explained by adsorbed water and for hydrogen by primary amine groups at the border of the structures or vacancies. A significant amount of oxygen can also be found in functional groups proven using FTIR and XPS measurements.

Figure 3b shows the FTIR spectrum of the product. There are multiple bands, which can be assigned to different absorptions which are characteristic for carbon nitrides in general. The sharp peak at 775 cm^{-1} can be ascribed to the out-of-plane bending mode of either triazine or heptazine rings. The fingerprint region between 1100 and 1700 cm^{-1} shows various absorption maxima for imide and nitride stretching vibrations. Around 1260 cm^{-1}, the characteristic band for the C−NH−C unit is found. The bands around 2170, 1720, and 1180 cm^{-1} indicate the presence of nitrile- or oxygen-containing functional groups such as C═O or C−OH. The bands at 3330 and 3130 cm^{-1} are related to NH-stretching vibrations.[14,15] To further confirm PTI as the product of the as-described synthesis, NMR and XPS experiments were conducted.

NMR spectroscopy is a powerful tool to identify the chemical structure of PTI and to exclude a heptazine-based structure. Up to now, most carbon nitrides were analyzed by solid state MAS-NMR spectroscopy[2,14,48,59,63] because of the vanishing solubility of carbon nitrides in common solvents. Unfortunately, compared to liquid-state NMR spectroscopy, this method is time-consuming and lacks resolution. For polymeric carbon nitride (melon), a heptazine-based carbon nitride, NMR spectra have been recorded in concentrated sulfuric acid.[64]

The ^{13}C NMR spectrum of PTI shown in Figure 3d,e is defined by several signals distributed in the region between 166.7 and 171.5 ppm. Signals in that region are typically observed for both triazine- and heptazine-based carbon nitride materials.[2,14,48,59,63] Therefore, the ^{15}N NMR spectrum is needed to assign the observed ^{13}C NMR signals to the triazine-based PTI. The carbon atoms in the triazine ring are located next to imide groups as well as primary and secondary amine groups. Also, nitrile- or oxygen-containing functional groups are observed in FTIR and XPS spectra and contribute to the shown NMR spectrum by slight shifts in this region. Figure S5a shows the solid state CPMAS ^{13}C NMR spectrum of PTI. It consists of two broad signals at 165.5 and 157.2 ppm. The observed shifts result by the stacking of the PTI planes in solid state. Also, solvent interaction has to be reconsidered. The ^{15}N NMR spectrum of PTI was collected in a heteronuclear multiband correlation experiment (Figure 3c). It consists of three signals at −212.4, −249.5, and −296.8 ppm. The first signal is assigned to the tertiary nitrogen atom in the outer ring of triazine or heptazine units in accordance to the literature.[14,15] The absence of a signal reported for heptazines in the region of −225 to −235 ppm suggests that no central heptazine nitrogen atom is present.[2] The signal at −249.5 ppm can be assigned to bridging
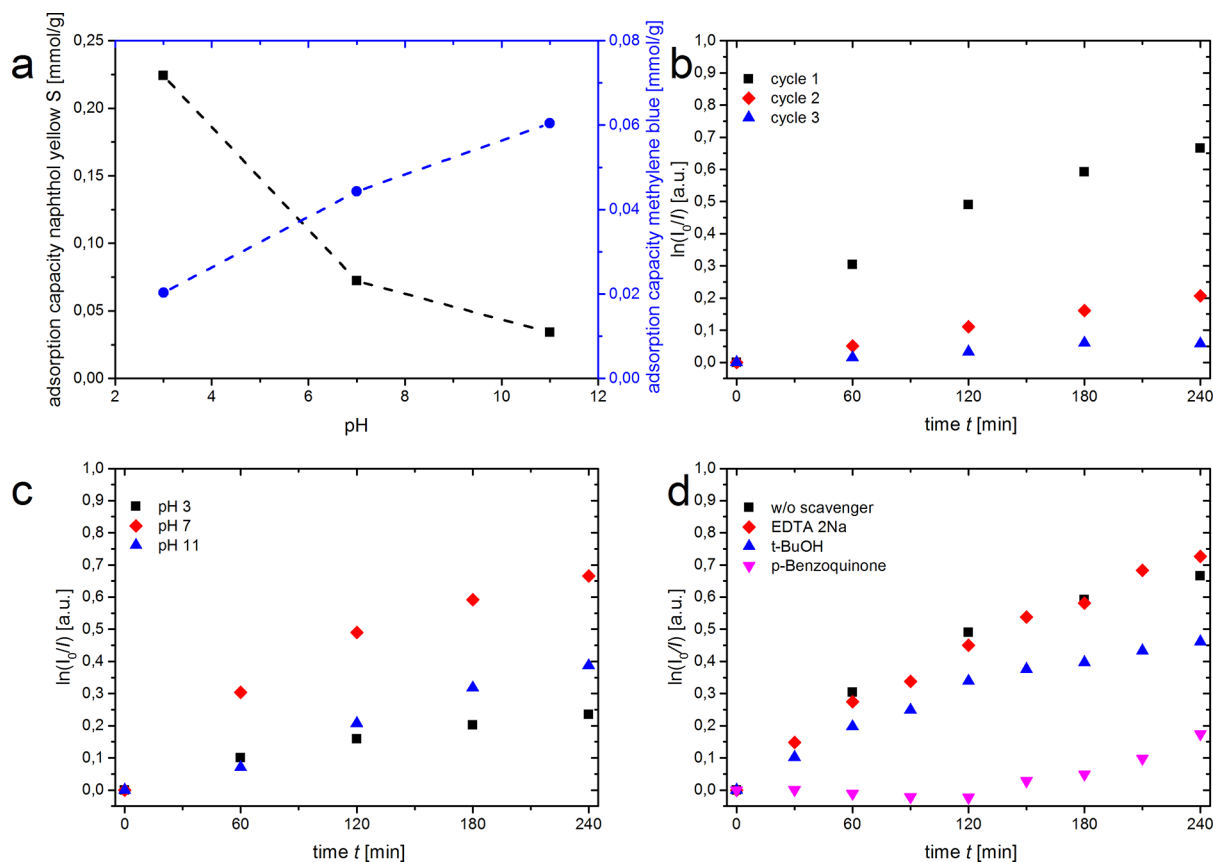
Figure 5. Adsorption capacity of PTI for the ionic dyes NYS (black squares) and MB (blue circles) at different pH values. PTI shows a higher capacity for the anionic NYS at low pH values because of charging of PTI by protonation. In contrast, the adsorption of cationic MB is increased at high pH values because of the charges formed because of deprotonation of PTI (a). Logarithmic plots of the intensity of the MB solution against the duration of the degradation in recycling experiments (b) as well as at different pH values (c). The intensity was determined at the absorption maximum at 664 nm. The reaction constants were determined by fitting the linear region at 120−240 min. Logarithmic plot of intensity of the MB solution against the duration of the degradation at pH 7. Different scavengers were used to determine the active species in the degradation process. It is shown that *p*-benzoquinone lowers the degradation rate for a certain time (d).

NH groups of PTI. The latter signal at −296.4 ppm is ascribed to the nitrogen atom in the amine groups. These assignments are confirmed by the correlated ^{1}H NMR spectrum, which shows three signals for the amine group centered at 6.52 ppm and one signal at 8.68 ppm for bridging imide groups. Figure S5b shows the solid state CPMAS ^{15}N NMR spectrum of PTI. Three main signals at −218.0, −241.5, and −292.6 ppm are present and confirm the liquid-state NMR.

XPS measurements are performed to analyze the PTI composition. Figure S6a shows the survey spectra of the PTI and demonstrates the corresponding C 1s and N 1s peaks. The deconvoluted XP spectra of C 1s and N 1s regions are shown in Figure 4. The deconvoluted C 1s peak (Figure 4a) demonstrates four components at binding energies (BEs) of 284.5, 285.3, 288.15, and 289.5 eV. These components correspond to the graphitic carbon, aliphatic carbon, C−N, and carboxylic groups, respectively. The dominant C 1s peak at 288.1 eV originates from sp^2, where the carbon atom bonds to N inside the triazine ring.[65,66] The contribution of the carbon groups at the BE of 289.5 eV is attributed to the hydroxyl and carboxylate groups and reveals oxidation of the surface during the electrochemical induced synthesis. The corresponding O peaks for the −OH and −COOH are observed at 531.1 and 532.1 eV, respectively (see O 1s peak in Figure S6b). Deconvoluted N 1s spectra presented in Figure 4b shows three peaks centered at 398.4, 399.6, and 400.7 eV assigned to

the sp^2 nitrogen in the triazine ring, bridging N atoms, and the primary amine groups, respectively.[12,65−67]

Thermogravimetric analysis shows the high temperature stability of PTI (Figure S7). With an increasing temperature, water desorbs, and at 100 °C, a plateau is reached independently of the surrounding atmosphere. At 300 °C, in an ambient atmosphere, a constant mass loss is observed, which we assume to be determined by the sublimation of PTI as well as the complete decomposition at higher temperatures. A complete mass loss is observed at 575 °C. In a nitrogen atmosphere, at 300 °C, significant mass loss is observed as well, but a second plateau is reached at 450 °C. This plateau may be reached because of further condensation of PTI. It is followed by further mass loss until a minimum of 2% residue mass is observed at 675 °C. In contrast to the measurements in the ambient atmosphere, a black residue remains.

The PL spectrum of PTI in NaOH at pH 12 indicates a distinct emission maximum at 425 nm at an excitation wavelength of 250 nm (Figure 4a). With an increasing excitation wavelength, a red shift is observed up to 447 nm. The red shift might be explained by electronic transitions which become unlikely at lower energies and are in general observed because of the changes in the electronic structure of PTI due to the deprotonation. This property is not observed for PTI in DMSO (shown in Figure S8a). The emission maximum only slightly varies around 443 nm. In both solvents, the emission

covers a large range of the visible spectrum, which makes PTI a promising material for UV and white-light LEDs. This property as well as the spontaneous dissolution of PTI in polar aprotic solvents [dimethylformamide, DMSO, N-methyl-2-pyrrolidone, dimethylacetamide] has been recently described by Miller et al.[60] In contrast to their reports, we do not observe any broadening of the emission with an increasing excitation wavelength of PTI neither in NaOH nor in DMSO. The full width at half-maximum (fwhm) found for the latter is around 120 nm independently of the excitation wavelength, while the former shows a narrower fwhm of around 100 nm. The PLE spectrum of PTI in NaOH solution shows a high intensity at 332 nm, as it has also been reported by Miller et al. Additionally, we observe a smaller maximum at 370 nm, whereas the reported maximum of few layer PTI nanosheets at 270 nm could not be observed in NaOH solution (Figure S8b). Raman scattering of water results in the maximum at 370 nm. In DMSO, the PLE maximum is found at 357 nm and only one peak is observed (Figure S8b). We explain the differences in the spectra by emphasizing the different mechanisms of the dissolution processes. In NaOH, PTI is deprotonated, and therefore, the electronic properties are influenced, whereas in DMSO, PTI is not chemically altered. The energy gap between the highest occupied molecular orbital and the lowest unoccupied molecular orbital of 3.28 eV is determined through a Tauc plot (Figure S9b), which was extracted from a diffuse reflectance spectrum (Figure S9a).

Photocatalytic Experiments. Prior to photocatalytic experiments, the adsorption of ionic dyes on PTI was investigated. The cationic dye MB and the anionic dye NYS were used. Because of charges generated by adjusting the pH value, the adsorption behavior of the ionic dyes is influenced. It was shown that MB adsorbs well at neutral (pH 7, capacity for MB: 0.04 mmol/g) and increased pH values (pH 11, capacity for MB: 0.06 mmol/g), but it has a small adsorption capacity at low pH values (pH 3, capacity for MB: 0.02 mmol/g). For NYS, in contrast, the adsorption at neutral (pH 7, capacity for NYS: 0.07 mmol/g) and increased pH values (pH 11, capacity for NYS: 0.03 mmol/g) is small compared to decreased pH values (pH 3, capacity for NYS: 0.22 mmol/g). Hence, we show that by adjusting the pH value in the experiment specific adsorption of charged molecules can be achieved. This property is important for the selectivity of the catalyst to bind specific molecules and influences the catalytic activity. Figure 5a shows the pH value-dependent adsorption capacity of PTI for MB and NYS. The adsorption capacity was determined at the equilibrium of the adsorption and desorption processes, which was reached after 60 min (Figure S10).

These experiments were followed by dye degradation experiments under illumination with a xenon lamp in combination with a water filter to exclude thermal effects. For NYS, no significant degradation was observed, therefore only the degradation of MB is described in the following section. The spectrum of the lamp used for the photocatalytic experiments is shown in Figure S11. The UV−vis spectra used to determine the intensity at the maximum at 664 nm as well as the references are shown in the Supporting Information (Figure S12).

Degradation of MB. The performed experiments prove the photocatalytic activity of PTI in the degradation process of MB. It was shown that degradation of MB could be observed for at least three cycles at neutral pH value (Figure 5b). However, it has to be conceded that the degradation rate decreases

significantly by a factor of 3 (cycle 1: $k_1 = 1.5 \times 10^{-3}$ min^{-1}, cycle 2: $k_2 = 0.8 \times 10^{-3}$ min^{-1}, and cycle 3: $k_3 = 0.4 \times 10^{-3}$ min^{-1}, k was determined using linear regression of the data points for 120, 180, and 240 min). Besides, it has also been shown that the pH value has a strong influence on the reaction rate constant. The logarithmic plots are shown in Figure 5c. At low pH values, the adsorption of MB is lowered (0.02 mmol/g at pH 3), whereas at high pH values (0.06 mmol/g at pH 11) a 3 times higher amount of dye can be adsorbed. The degradation rates determined at pH 3, pH 7, and pH 11 are $k_{pH3} = 0.6 \times 10^{-3}$ min^{-1}, $k_{pH7} = 1.5 \times 10^{-3}$ min^{-1}, and $k_{pH11} = 1.5 \times 10^{-3}$ min^{-1}. It can be observed that by adjusting the pH the degradation rate can be influenced. In comparison to the degradation rates at pH 7 and pH 11, the rate at pH 3 is lowered by the factor of 2.5, which is in good agreement with the observed lower adsorption capacity.

Investigation of Different Active Species. Different scavenger molecules have been added to the photocatalytic experiments to investigate the active species in the degradation process. The influence of holes, hydroxyl radicals, as well as superoxide radicals was determined by adding EDTA-2Na, t-butanol, and p-benzoquinone, respectively. As shown in Figure 5d at pH 7, the addition of EDTA-2Na does not have any influence on the degradation rate ($k_{EDTA-2Na} = 2.3 \times 10^{-3}$ min^{-1}) of MB. Thus, it is assumed that hydroxyl radicals are not the active species in the degradation process. Adding t-BuOH to the experiment results in a slightly lowered degradation rate ($k_{t-BuOH} = 1.0 \times 10^{-3}$ min^{-1}). In contrast, p-benzoquinone has a significant influence. It is observed that for nearly 2 h of illumination, no degradation is observed and no reaction constant could be determined. Instead, a shift in the absorption of p-benzoquinone is observed. After 2 h, no further shifting is occurring and the degradation of MB takes place. The reaction constant in this regime is in the same range as the degradation without any scavenger. Therefore, it is concluded that superoxide radicals are the main active species and that these radicals only react with MB after the reaction with p-benzoquinone is completed.

■ CONCLUSIONS

In summary, this work describes a new approach for the synthesis of a triazine-based carbon nitride material which we identified as PTI. This approach has its origin in a synthesis described for triazine-based graphitic carbon nitride by Lu et al.[59] Our modification of the synthesis approach yields PTI, which we identified with the help of several characterization techniques, for example, XPS, powder XRD, FTIR, and two-dimensional liquid-state NMR spectroscopy. The latter is a rarity for carbon nitride materials because the solubility in common solvents is low. Because of this synthesis approach, oxygen-containing functional groups are incorporated in the structure of PTI resulting in the possibility of protonation and deprotonation. This charging leads to an increased solubility. The as-obtained PTI has a comparably high specific surface area and also shows high-temperature stability. We showed the photocatalytic properties of PTI in the degradation process of ionic dyes and discussed the influence of the pH value in this process, especially in the adsorption process. We were able to influence the adsorption capacity of PTI for different molecules by adjusting the pH value. The addition of different scavengers showed that superoxide radicals are the main active species in the presented degradation experiments.

EXPERIMENTAL SECTION

Chemicals. Melamine (99%) was purchased from Sigma-Aldrich, sodium hydroxide (97%) was purchased from Grüssing GmbH, MB was purchased from Merck Chemicals GmbH, NYS was purchased from Alfa Aesar, *tert*-butanol (99%) was purchased from Grüssing GmbH, EDTA-2Na (>98.5%) was purchased from Sigma-Aldrich, *para*-benzoquinone was purchased from Sigma-Aldrich and recrystallized in 2-propanol, and terephthalic acid (98%) was purchased from Sigma-Aldrich.

Synthesis of PTI. Melamine (945 mg; 7.5 mmol) was dissolved in 100 mL of demineralized water at 65 °C under vigorous stirring. In a three electrode setup with a reference electrode (Ag/AgCl/KCl), counter electrode (platinum), and working electrode (platinum), a voltage of 5 V was applied for 6 h at 65 °C without stirring. The distance between counter and working electrodes was 0.5 cm. The current increased linearly during the reaction from 1 to 200 mA, and the formation of gases at the electrode surfaces increased as well. After 6 h, the product was obtained in a brownish suspension. A scheme of the setup is shown in Figure S1.

The suspension was centrifuged for 5 min at 7500 rpm (13 206 rcf). The supernatant was discarded. The residue was dispersed in 30 mL of hot demineralized water. This process was repeated three times. The washed product was freeze-dried and obtained as a pale yellowish powder. This synthesis approach and the following washing procedure yield in average 55 mg of PTI.

Photocatalytic Experiments. The catalyst material (50 mg) was dispersed in 100 mL of either a 10 mg/L MB or a 60 mg/L NYS solution and stirred for 1 h in the dark to set an adsorption/desorption equilibrium. As a light source, a 300 W xenon lamp (UXL-302-O) combined with a water filter to avoid heating effects by infrared radiation was used. Aliquots of 4 mL were taken every 60 min (or 30 min for scavenger experiments). The aliquots were centrifuged once at 11 000 rpm (28 408 rcf) to remove the catalyst material. The supernatant was filtered using a hydrophilic syringe filter (nylon, 0.2 μm pore size).

The pH value was adjusted in the experiments by the addition of hydrochloric acid or sodium hydroxide before the addition of the catalyst. All of the measurements were controlled by performing the same experiments without illumination as well as without the catalyst.

To identify the reactive species in the degradation process, experiments were conducted as described above, but *tert*-butanol (10 vol %), EDTA-2Na (10 mM), or *para*-benzoquinone (10 mM) was added to the experiment.

ASSOCIATED CONTENT

Ⓢ Supporting Information

The Supporting Information is available free of charge on the ACS Publications website at DOI: 10.1021/acsomega.8b00294.

Experimental methods, scheme of the experimental setup, formation of hydroxyl radicals during the reaction, BET measurements, SEM and TEM images, solid state ^{13}C and ^{15}N NMR spectra, full XP spectrum and deconvoluted O 1s peak, thermogravimetric analysis of PTI in ambient and nitrogen atmosphere, UV−vis spectra of PTI in solid state, resulting Tauc plot and UV−vis spectra in DMSO, xenon lamp spectrum, and UV−vis spectra of aliquots taken during dye degradation (PDF)

AUTHOR INFORMATION

Corresponding Author

*E-mail: klinke@chemie.uni-hamburg.de.

ORCID Ⓞ

Heshmat Noei: 0000-0003-1294-3527
Christian Klinke: 0000-0001-8558-7389

Notes

The authors declare no competing financial interest.

REFERENCES

(1) Wang, X.; Maeda, K.; Thomas, A.; Takanabe, K.; Xin, G.; Carlsson, J. M.; Domen, K.; Antonietti, M. A metal-free polymeric photocatalyst for hydrogen production from water under visible light. *Nat. Mater.* **2009**, *8*, 76−80.

(2) Lotsch, B. V.; Döblinger, M.; Sehnert, J.; Seyfarth, L.; Senker, J.; Oeckler, O.; Schnick, W. Unmasking Melon by a Complementary Approach Employing Electron Diffraction, Solid-State NMR Spectroscopy, and Theoretical Calculations - Structural Characterization of a Carbon Nitride Polymer. *Chem.—Eur. J.* **2007**, *13*, 4969−4980.

(3) Jürgens, B.; Irran, E.; Senker, J.; Kroll, P.; Müller, H.; Schnick, W. Melem (2,5,8-Triamino-tri-*s*-triazine), an Important Intermediate during Condensation of Melamine Rings to Graphitic Carbon Nitride: Synthesis, Structure Determination by X-ray Powder Diffractometry, Solid-State NMR, and Theoretical Studies. *J. Am. Chem. Soc.* **2003**, *125*, 10288−10300.

(4) Liu, J.; Zhang, T.; Wang, Z.; Dawson, G.; Chen, W. Simple pyrolysis of urea into graphitic carbon nitride with recyclable adsorption and photocatalytic activity. *J. Mater. Chem.* **2011**, *21*, 14398−14401.

(5) Zhang, Y.; Pan, Q.; Chai, G.; Liang, M.; Dong, G.; Zhang, Q.; Qiu, J. Synthesis and luminescence mechanism of multicolor-emitting g-C$_3$N$_4$ nanopowders by low temperature thermal condensation of melamine. *Sci. Rep.* **2013**, *3*, 1943.

(6) Yan, S. C.; Li, Z. S.; Zou, Z. G. Photodegradation Performance of g-C$_3$N$_4$ Fabricated by Directly Heating Melamine. *Langmuir* **2009**, *25*, 10397−10401.

(7) Wang, X.; Maeda, K.; Chen, X.; Takanabe, K.; Domen, K.; Hou, Y.; Fu, X.; Antonietti, M. Polymer Semiconductors for Artificial Photosynthesis: Hydrogen Evolution by Mesoporous Graphitic Carbon Nitride with Visible Light. *J. Am. Chem. Soc.* **2009**, *131*, 1680−1681.

(8) Bai, X.; Yan, S.; Wang, J.; Wang, L.; Jiang, W.; Wu, S.; Sun, C.; Zhu, Y. A simple and efficient strategy for the synthesis of a chemically tailored g-C$_3$N$_4$ material. *J. Mater. Chem. A* **2014**, *2*, 17521−17529.

(9) Zhang, Y.; Liu, J.; Wu, G.; Chen, W. Porous graphitic carbon nitride synthesized via direct polymerization of urea for efficient sunlight-driven photocatalytic hydrogen production. *Nanoscale* **2012**, *4*, 5300−5303.

(10) Liu, X.; Luo, L.; Ding, Y.; Wu, Q.; Wei, Y.; Ye, D. A highly sensitive method for determination of guanine, adenine and epinephrine using poly-melamine film modified glassy carbon electrode. *J. Electroanal. Chem.* **2012**, *675*, 47−53.

(11) Baskar, S.; Liao, C.-W.; Chang, J.-L.; Zen, J.-M. Electrochemical synthesis of electroactive poly(melamine) with mechanistic explanation and its applicability to functionalize carbon surface to prepare nanotube-nanoparticles hybrid. *Electrochim. Acta* **2013**, *88*, 1−5.

(12) Chen, Z.; Savateev, A.; Pronkin, S.; Papaefthimiou, V.; Wolff, C.; Willinger, M. G.; Willinger, E.; Neher, D.; Antonietti, M.; Dontsova, D. "The Easier the Better" Preparation of Efficient Photocatalysts − Metastable Poly(heptazine imide) Salts. *Adv. Mater.* **2017**, *29*, 1700555.

(13) Savateev, A.; Pronkin, S.; Epping, J. D.; Willinger, M. G.; Wolff, C.; Neher, D.; Antonietti, M.; Dontsova, D. Potassium Poly(heptazine imides) from Aminotetrazoles: Shifting Band Gaps of Carbon Nitride-like Materials for More Efficient Solar Hydrogen and Oxygen Evolution. *ChemCatChem* **2017**, *9*, 167−174.

(14) Wirnhier, E.; Döblinger, M.; Gunzelmann, D.; Senker, J.; Lotsch, B. V.; Schnick, W. Poly(triazine imide) with Intercalation of Lithium and Chloride Ions $[(C_3N_3)_2(NH_xLi_{1-x})_3 \cdot LiCl]$: A Crystalline 2D Carbon Nitride Network. *Chem.—Eur. J.* **2011**, *17*, 3213−3221.

(15) Schwinghammer, K.; Tuffy, B.; Mesch, M. B.; Wirnhier, E.; Martineau, C.; Taulelle, F.; Schnick, W.; Senker, J.; Lotsch, B. V. Triazine-based Carbon Nitrides for Visible-Light-Driven Hydrogen Evolution. *Angew. Chem., Int. Ed.* **2013**, *52*, 2435−2439.

(16) McDermott, E. J.; Wirnhier, E.; Schnick, W.; Virdi, K. S.; Scheu, C.; Kauffmann, Y.; Kaplan, W. D.; Kurmaev, E. Z.; Moewes, A. Band Gap Tuning in Poly(triazine imide), a Nonmetallic Photocatalyst. *J. Phys. Chem. C* **2013**, *117*, 8806−8812.

(17) Bojdys, M. J.; Severin, N.; Rabe, J. P.; Cooper, A. I.; Thomas, A.; Antonietti, M. Exfoliation of Crystalline 2D Carbon Nitride: Thin Sheets, Scrolls and Bundles via Mechanical and Chemical Routes. *Macromol. Rapid Commun.* **2013**, *34*, 850−854.

(18) Lee, W.-R.; Jun, Y.-S.; Park, J.; Stucky, G. D. Crystalline poly(triazine imide) based g-CN as an efficient electrocatalyst for counter electrodes of dye-sensitized solar cells using a triiodide/iodide redox electrolyte. *J. Mater. Chem. A* **2015**, *3*, 24232−24236.

(19) Kessler, F. K.; Zheng, Y.; Schwarz, D.; Merschjann, C.; Schnick, W.; Wang, X.; Bojdys, M. J. Functional carbon nitride materials − design strategies for electrochemical devices. *Nat. Rev. Mater.* **2017**, *2*, 17030.

(20) Zheng, Y.; Lin, L.; Ye, X.; Guo, F.; Wang, X. Helical Graphitic Carbon Nitrides with Photocatalytic and Optical Activities. *Angew. Chem., Int. Ed.* **2014**, *53*, 11926−11930.

(21) Wang, K.; Li, Q.; Liu, B.; Cheng, B.; Ho, W.; Yu, J. Sulfur-doped g-C₃N₄ with enhanced photocatalytic CO₂-reduction performance. *Appl. Catal., B* **2015**, *176−177*, 44−52.

(22) Dong, G.; Zhang, L. Porous structure dependent photoreactivity of graphitic carbon nitride under visible light. *J. Mater. Chem.* **2012**, *22*, 1160−1166.

(23) Niu, P.; Yang, Y.; Yu, J. C.; Liu, G.; Cheng, H.-M. Switching the selectivity of the photoreduction reaction of carbon dioxide by controlling the band structure of a g-C₃N₄ photocatalyst. *Chem. Commun.* **2014**, *50*, 10837−10840.

(24) Mao, J.; Peng, T.; Zhang, X.; Li, K.; Ye, L.; Zan, L. Effect of graphitic carbon nitride microstructures on the activity and selectivity of photocatalytic CO₂ reduction under visible light. *Catal. Sci. Technol.* **2013**, *3*, 1253−1260.

(25) Xia, P.; Zhu, B.; Yu, J.; Cao, S.; Jaroniec, M. Ultra-thin nanosheet assemblies of graphitic carbon nitride for enhanced photocatalytic CO₂ reduction. *J. Mater. Chem. A* **2017**, *5*, 3230−3238.

(26) Li, X.; Masters, A. F.; Maschmeyer, T. Polymeric carbon nitride for solar hydrogen production. *Chem. Commun.* **2017**, *53*, 7438−7446.

(27) Wu, P.; Wang, J.; Zhao, J.; Guo, L.; Osterloh, F. E. High alkalinity boosts visible light driven H₂ evolution activity of g-C₃N₄ in aqueous methanol. *Chem. Commun.* **2014**, *50*, 15521−15524.

(28) Lau, V. W.-H.; Mesch, M. B.; Duppel, V.; Blum, V.; Senker, J.; Lotsch, B. V. Low-Molecular-Weight Carbon Nitrides for Solar Hydrogen Evolution. *J. Am. Chem. Soc.* **2015**, *137*, 1064−1072.

(29) Martin, D. J.; Qiu, K.; Shevlin, S. A.; Handoko, A. D.; Chen, X.; Guo, Z.; Tang, J. Highly Efficient Photocatalytic H₂ Evolution from Water using Visible Light and Structure-Controlled Graphitic Carbon Nitride. *Angew. Chem., Int. Ed.* **2014**, *53*, 9240−9245.

(30) Chang, F.; Xie, Y.; Li, C.; Chen, J.; Luo, J.; Hu, X.; Shen, J. A facile modification of *g*-C₃N₄ with enhanced photocatalytic activity for degradation of methylene blue. *Appl. Surf. Sci.* **2013**, *280*, 967−974.

(31) She, X.; Xu, H.; Xu, Y.; Yan, J.; Xia, J.; Xu, L.; Song, Y.; Jiang, Y.; Zhang, Q.; Li, H. Exfoliated graphene-like carbon nitride in organic solvents: enhanced photocatalytic activity and highly selective and sensitive sensor for the detection of trace amounts of Cu²⁺. *J. Mater. Chem. A* **2014**, *2*, 2563−2570.

(32) Bai, X.; Wang, L.; Zong, R.; Zhu, Y. Photocatalytic Activity Enhanced via g-C₃N₄ Nanoplates to Nanorods. *J. Phys. Chem. C* **2013**, *117*, 9952−9961.

(33) Lee, E. Z.; Jun, Y.-S.; Hong, W. H.; Thomas, A.; Jin, M. M. Cubic Mesoporous Graphitic Carbon(IV) Nitride: An All-in-One Chemosensor for Selective Optical Sensing of Metal Ions. *Angew. Chem., Int. Ed.* **2010**, *49*, 9706−9710.

(34) Tian, J.; Liu, Q.; Asiri, A. M.; Al-Youbi, A. O.; Sun, X. Ultrathin Graphitic Carbon Nitride Nanosheet: A Highly Efficient Fluorosensor for Rapid, Ultrasensitive Detection of Cu²⁺. *Anal. Chem.* **2013**, *85*, 5595−5599.

(35) Cheng, C.; Huang, Y.; Tian, X.; Zheng, B.; Li, Y.; Yuan, H.; Xiao, D.; Xie, S.; Choi, M. M. F. Electrogenerated Chemiluminescence Behavior of Graphite-like Carbon Nitride and Its Application in Selective Sensing Cu²⁺. *Anal. Chem.* **2012**, *84*, 4754−4759.

(36) Ma, T. Y.; Tang, Y.; Dai, S.; Qiao, S. Z. Proton-Functionalized Two-Dimensional Graphitic Carbon Nitride Nanosheet: An Excellent Metal-/Label-free Biosensing Platform. *Small* **2014**, *10*, 2382−2389.

(37) Liu, J.; Wang, H.; Antonietti, M. Graphitic carbon nitride "reloaded": emerging applications beyond (photo)catalysis. *Chem. Soc. Rev.* **2016**, *45*, 2308−2326.

(38) Wang, Y.; Wang, X.; Antonietti, M. Polymeric Graphitic Carbon Nitride as a Heterogeneous Organocatalyst: From Photochemistry to Multipurpose Catalysis to Sustainable Chemistry. *Angew. Chem., Int. Ed.* **2012**, *51*, 68−89.

(39) Chen, X.; Zhang, J.; Fu, X.; Antonietti, M.; Wang, X. Fe-g-C₃N₄-Catalyzed Oxidation of Benzene to Phenol Using Hydrogen Peroxide and Visible Light. *J. Am. Chem. Soc.* **2009**, *131*, 11658−11659.

(40) Su, F.; Mathew, S. C.; Lipner, G.; Fu, X.; Antonietti, M.; Blechert, S.; Wang, X. mpg-C₃N₄-Catalyzed Selective Oxidation of Alcohols Using O₂ and Visible Light. *J. Am. Chem. Soc.* **2010**, *132*, 16299−16301.

(41) Su, F.; Mathew, S. C.; Möhlmann, L.; Antonietti, M.; Wang, X.; Blechert, S. Aerobic Oxidative Coupling of Amines by Carbon Nitride Photocatalysis with Visible Light. *Angew. Chem., Int. Ed.* **2011**, *50*, 657−660.

(42) Kurpil, B.; Kumru, B.; Heil, T.; Antonietti, M.; Savateev, A. Carbon nitride creates thioamides in high yields by the photocatalytic Kindler reaction. *Green Chem.* **2018**, *20*, 838−842.

(43) Ong, W.-J.; Tan, L.-L.; Ng, Y. H.; Yong, S.-T.; Chai, S.-P. Graphitic Carbon Nitride (g-C₃N₄)-Based Photocatalysts for Artificial Photosynthesis and Environmental Remediation: Are We a Step Closer To Achieving Sustainability? *Chem. Rev.* **2016**, *116*, 7159−7329.

(44) Lu, Y.-C.; Chen, J.; Wang, A.-J.; Bao, N.; Feng, J.-J.; Wang, W.; Shao, L. Facile synthesis of oxygen and sulfur co-doped graphitic carbon nitride fluorescent quantum dots and their application for mercury(II) detection and bioimaging. *J. Mater. Chem. C* **2015**, *3*, 73−78.

(45) Raziq, F.; Qu, Y.; Zhang, X.; Humayun, M.; Wu, J.; Zada, A.; Yu, H.; Sun, X.; Jing, L. Enhanced Cocatalyst-Free Activities for Photocatalytic Fuel Production of g-C₃N₄ by Trapping Holes and Transferring Electrons. *J. Phys. Chem. C* **2016**, *120*, 98−107.

(46) Hu, S.; Ma, L.; You, J.; Li, F.; Fan, Z.; Wang, F.; Liu, D.; Gui, J. A Simple and efficient method to prepare a phosphorus modified g-C₃N₄ visible light photocatalyst. *RSC Adv.* **2014**, *4*, 21657−21663.

(47) Han, Q.; Hu, C.; Zhao, F.; Zhang, Z.; Chen, N.; Qu, L. One-step preparation of iodine-doped graphitic carbon nitride nanosheets as efficient photocatalysts for visible light water splitting. *J. Mater. Chem. A* **2015**, *3*, 4612−4619.

(48) Zhang, J.; Chen, X.; Takanabe, K.; Maeda, K.; Domen, K.; Epping, J. D.; Fu, X.; Antonietti, M.; Wang, X. Synthesis of a Carbon Nitride Structure for Visible-Light Catalysis by Copolymerization. *Angew. Chem., Int. Ed.* **2010**, *49*, 441−444.

(49) Zhang, Y.; Schnepp, Z.; Cao, J.; Ouyang, S.; Li, Y.; Ye, J.; Liu, S. Biopolymer-activated graphitic carbon nitride towards a sustainable photocathode material. *Sci. Rep.* **2013**, *3*, 2163.

(50) Yang, Z.; Zhang, Y.; Schnepp, Z. Soft and hard templating of graphitic carbon nitride. *J. Mater. Chem. A* **2015**, *3*, 14081−14092.

(51) Yan, H. Soft-templating synthesis of mesoporous graphitic carbon nitride with enhanced photocatalytic H_2 evolution under visible light. *Chem. Commun.* **2012**, *48*, 3430−3432.

(52) Shiraishi, Y.; Kofuji, Y.; Kanazawa, S.; Sakamoto, H.; Ichikawa, S.; Tanaka, S.; Hirai, T. Platinum nanoparticles strongly associated with graphitic carbon nitride as efficient co-catalysts for photocatalytic hydrogen evolution under visible light. *Chem. Commun.* **2014**, *50*, 15255−15258.

(53) Wang, Z.; Wei, J.; Liu, G.; Zhou, Y.; Han, K.; Ye, H. G-C_3N_4-coated activated carbon-supported Pd catalysts for 4-CBA hydrogenation: effect of nitrogen species. *Catal. Sci. Technol.* **2015**, *5*, 3926−3930.

(54) Zang, Y.; Li, L.; Xu, Y.; Zuo, Y.; Li, G. Hybridization of brookite TiO_2 with g-C_3N_4: a visible-light-driven photocataylst for As^{3+} oxidation, MO degradation and water splitting for hydrogen evolution. *J. Mater. Chem. A* **2014**, *2*, 15774−15780.

(55) Cheng, N.; Tian, J.; Liu, Q.; Ge, C.; Qusti, A. H.; Asiri, A. M.; Al-Youbi, A. O.; Sun, X. Au-Nanoparticle-Loaded Graphitic Carbon Nitride Nanosheets: Green Photocatalytic Synthesis and Application toward the Degradation of Organic Pollutants. *ACS Appl. Mater. Interfaces* **2013**, *5*, 6815−6819.

(56) Ge, L.; Zuo, F.; Liu, J.; Ma, Q.; Wang, C.; Sun, D.; Bartels, L.; Feng, P. Synthesis and Efficient Visible Light Photocatalytic Hydrogen Evolution of Polymeric g-C_3N_4 Coupled with CdS Quantum Dots. *J. Phys. Chem. C* **2012**, *116*, 13708−13714.

(57) Cui, W.; Li, J.; Dong, F.; Sun, Y.; Jiang, G.; Cen, W.; Lee, S. C.; Wu, Z. Highly Efficient Perfomance and Conversion Pathway of Photocatalytic NO Oxidation on SrO-Clusters@Amorphous Carbon Nitride. *Environ. Sci. Technol.* **2017**, *51*, 10682−10690.

(58) Lau, V. W.-H.; Klose, D.; Kasap, H.; Podjaski, F.; Pignié, M.-C.; Reisner, E.; Jeschke, G.; Lotsch, B. V. Dark Photocatalysis: Storage of Solar Energy in Carbon Nitride for Time-Delayed Hydrogen Generation. *Angew. Chem., Int. Ed.* **2017**, *56*, 510−514.

(59) Lu, Q.; Deng, J.; Hou, Y.; Wang, H.; Li, H.; Zhang, Y. One-step electrochemical synthesis of ultrathin graphitic carbon nitride nanosheets and their application to the detection of uric acid. *Chem. Commun.* **2015**, *51*, 12251−12253.

(60) Miller, T. S.; Suter, T. M.; Telford, A. M.; Picco, L.; Payton, O. D.; Russell-Pavier, F.; Cullen, P. L.; Sella, A.; Shaffer, M. S. P.; Nelson, J.; Tileli, V.; McMillan, P. F.; Howard, C. A. Single Crystal, Luminescent Carbon Nitride Nanosheets Formed by Spontaneous Dissolution. *Nano Lett.* **2017**, *177*, 5891−5896.

(61) Lu, J.; Yang, J.-X.; Wang, J.; Lim, A.; Wang, S.; Loh, K. P. One-Pot Synthesis of Fluorescent Carbon Nanoribbons, Nanoparticles, and Graphene by the Exfoliation of Graphite in Ionic Liquids. *ACS Nano* **2009**, *3*, 2367−2375.

(62) Ham, Y.; Maeda, K.; Cha, D.; Takanabe, K.; Domen, K. Synthesis and Photocatalytic Activity of Poly(triazine imide). *Chem.—Asian J.* **2013**, *8*, 218−224.

(63) Mesch, M. B.; Bärwinkel, K.; Krysiak, Y.; Martineau, C.; Taulelle, F.; Neder, R. B.; Kolb, U.; Senker, J. Solving the Hydrogen and Lithium Substructure of Poly(triazine imide)/LiCl Using NMR Crystallography. *Chem.—Eur. J.* **2016**, *22*, 16878−16890.

(64) Zhou, Z.; Wang, J.; Yu, J.; Shen, Y.; Li, Y.; Liu, A.; Liu, S.; Zhang, Y. Dissolution and Liquid Crystals Phase of 2D Polymeric Carbon Nitride. *J. Am. Chem. Soc.* **2015**, *137*, 2179−2182.

(65) Schwinghammer, K.; Mesch, M. B.; Duppel, V.; Ziegler, C.; Senker, J.; Lotsch, B. V. Crystalline Carbon Nitride Nanosheets for Improved Visible-Light Hydrogen Evolution. *J. Am. Chem. Soc.* **2014**, *136*, 1730−1733.

(66) Algara-Siller, G.; Severin, N.; Chong, S. Y.; Björkman, T.; Palgrave, R. G.; Laybourn, A.; Antonietti, M.; Khimyak, Y. Z.; Krasheninnikov, A. V.; Rabe, J. P.; Kaiser, U.; Cooper, A. I.; Thomas, A.; Bojdys, M. J. Triazine-Based Graphitic Carbon Nitride: a Two-Dimensional Semiconductor. *Angew. Chem., Int. Ed.* **2014**, *53*, 7450−7455.

(67) Stierle, A.; Keller, T.; Noei, H.; Vonk, V.; Röhlsberger, R. DESY NanoLab. *J. Large-Scale Res. Facil.* **2016**, *2*, A76.